

Trapped-ion toolbox to simulate quantum Otto heat engines

Rogério Jorge de Assis  ^{1,*} Ciro Micheletti Diniz  ^{1,†} Norton Gomes de Almeida  ^{2,‡} and Celso J. Villas Bôas  ^{1,§}

¹*Departamento de Física, Universidade Federal de São Carlos, Rodovia Washington Luís, km 235 - SP-310, 13565-905 São Carlos, SP, Brasil*

²*Instituto de Física, Universidade Federal de Goiás, Avenida Esperança s/n, Câmpus Samambaia, 74.690-900, Goiânia - GO, Brasil*

We present a scheme that utilizes an ion confined within a bi-dimensional trap to simulate a quantum Otto heat engine whose working substance is a two-level system. In this scheme, the electronic component of the ion (the two-level system) can interact with effective heat reservoirs of different types. We specifically focus on effective thermal reservoirs (those with positive temperatures), effective heat reservoirs with apparent negative temperatures, and effective squeezed thermal reservoirs. We show how to generate these effective reservoirs and provide numerical results to illustrate the applicability of the presented scheme. Finally, considering the same types of effective heat reservoirs, we briefly discuss the simulation of a quantum Otto heat engine where a quantum harmonic oscillator serves as the working substance.

I. INTRODUCTION

In recent decades, researchers have been actively working on formulating a theory that integrates thermodynamics with quantum mechanics, which has come to be known as quantum thermodynamics [1, 2]. Several studies in this area focus on investigating the so-called quantum heat engines: heat engines in which the working substance is a quantum system [3–44]. When studying quantum heat engines, a natural question is whether quantum resources can improve their performance. Addressing this question, Ref. [11] revealed that a quantum Otto heat engine (QOHE) with a quantum harmonic oscillator as its working substance can achieve higher efficiencies when, instead of a conventional thermal reservoir (a heat reservoir with a positive temperature), its heat source is a squeezed thermal reservoir. Furthermore, the authors showed that the efficiency of the corresponding QOHE can surpass the Carnot efficiency obtained from the temperatures of the thermal reservoirs before squeezing the hottest one, which is the maximum efficiency achievable by a heat engine operating solely with thermal reservoirs. Following this, Ref. [19] presented an experimental realization of such a QOHE. Employing a two-level system as the working substance, Ref. [37] demonstrated that a squeezed thermal reservoir can increase the efficiency of the QOHE beyond the Carnot efficiency (before squeezing) even when it operates with irreversible unitary strokes. Here we are referring to the concept of irreversibility from quantum thermodynamics perspective, see Ref. [45]. Using the same working substance but now considering a heat reservoir with an apparent negative temperature as the heat source, Ref. [28] showed that the efficiency of the QOHE can exceed the

Otto efficiency when the unitary strokes are irreversible. The potential of using different types of heat reservoirs to improve engine efficiency is the motivation of the present paper.

We present in this paper a scheme that employs an ion confined in a bi-dimensional trap to simulate QOHE whose working substance is a two-level system. The proposed scheme allows the two-level system to operate with different kinds of effective heat reservoirs. Here we focus on effective thermal reservoirs, effective heat reservoirs with apparent negative temperatures, and effective squeezed thermal reservoirs. We begin in Sec. II by describing the physical model employed to simulate the QOHE whose working substance is the two-level system. Then, in Secs. III and IV, we provide an overview of the unitary and non-unitary strokes that give rise to the quantum Otto cycle. In Sec. IV, we present the procedure for generating the effective heat reservoirs for the two-level system. Next, in Sec. V, we describe the quantum Otto cycle and provide the engine efficiency when it operates as a heat engine. In Sec. VI, we show some numerical results. Additionally, in Sec. VII, we discuss the simulation of a QOHE with a quantum harmonic oscillator as the working substance, considering the same types of effective heat reservoirs as above. Finally, in Sec. VIII, we present our conclusions.

II. PHYSICAL MODEL

The physical model we consider here consists of an ion within a two-dimensional trap, allowing it to oscillate harmonically along both the x - and y -axes. We assume here that two energy levels approximately describe the electronic structure of the ion. Furthermore, we admit that the ion can interact (through its dipole moment) with the electric field of four distinct laser beams: two propagating along the x -direction and two along the y -direction. The Hamiltonian that describes this system at

* rjdeassis@gmail.com

† ciromd@outlook.com.br

‡ norton@ufg.br

§ celsov@df.ufscar.br

time t has the form

$$H^{SP}(t) = H_e^{SP} + H_m^{SP} + H_{int}^{SP}(t), \quad (1)$$

with H_e^{SP} , H_m^{SP} , and $H_{int}^{SP}(t)$ being the electronic, the motional, and the interaction Hamiltonian, respectively. The superscript “ SP ” indicates that these Hamiltonians are in the Schrödinger picture. Explicitly, the Hamiltonians H_e^{SP} and H_m^{SP} are given by

$$H_e^{SP} = \frac{\hbar\omega_e}{2}\sigma_z \quad (2)$$

and

$$H_m^{SP} = \sum_{\alpha=x,y} \hbar\omega_m a_{\alpha}^{\dagger} a_{\alpha}, \quad (3)$$

where ω_e is the electronic frequency, σ_z is the z -Pauli matrix, ω_m is the motional frequency of the ion along the x - and y -axes (treated as equal for both axes to simplify the model), and a_{α} (a_{α}^{\dagger}) is the respective annihilation (creation) operator, with α being x or y . Considering the Lamb-Dicke regime, where the Lamb-Dicke parameter λ (assumed to be the same for all lasers for simplicity) satisfies $\lambda[\text{tr}_m(a_{\alpha}^{\dagger} a_{\alpha})]^{1/2} \ll 1$, the interaction Hamiltonian can be written as [46]

$$H_{int}^{SP}(t) = \sum_{\alpha=x,y} \sum_{l=1}^2 \frac{\hbar\Omega_{\alpha,l}}{2} (\sigma_{ge} + \sigma_{ge}^{\dagger}) \times \left\{ 1 + i\lambda(a_{\alpha} e^{-i\omega_m t} + a_{\alpha}^{\dagger} e^{i\omega_m t}) e^{-i(\omega_{\alpha,l}^L t - \phi)} + \text{H.c.} \right\}, \quad (4)$$

where $\Omega_{\alpha,l}$ is the (α,l) -Rabi frequency, $\sigma_{ge} = |g\rangle\langle e|$ ($\sigma_{ge}^{\dagger} = |e\rangle\langle g|$) is the lowering (raising) operator, with $|g\rangle$ ($|e\rangle$) corresponding to the fundamental (excited) electronic eigenstate, λ is the Lamb-Dicke parameter, $\omega_{\alpha,l}^L$ is the (α,l) -laser frequency, and ϕ is the initial phase of the lasers (set to the same value for all lasers for convenience). We assume that the dynamics of the ion state $\rho^{SP}(t)$ is that of a weak interaction with the reservoir within the Born-Markov approximations, and therefore obeys the master equation

$$\dot{\rho}^{SP}(t) = \frac{1}{i\hbar} [H^{SP}(t), \rho^{SP}(t)] + \sum_{\alpha=x,y} \frac{\kappa}{2} D[a_{\alpha}] \rho^{SP}(t), \quad (5)$$

in which κ is the motional decay rate (also considered the same for the x - and y -directions, for simplicity) and $D[a_{\alpha}] \rho^{SP}(t) = 2a_{\alpha} \rho^{SP}(t) a_{\alpha}^{\dagger} - a_{\alpha}^{\dagger} a_{\alpha} \rho^{SP}(t) - \rho^{SP}(t) a_{\alpha}^{\dagger} a_{\alpha}$. As can be seen, we neglect the electronic decay, which is a reasonable assumption when it is much smaller than κ . This regime can be achieved, for instance, by considering long-lived metastable electronic states.

To simulate the QOHE described below, we switch to a rotating frame defined by the unitary transformation

$$R(t) = e^{-i(\omega t/2)\sigma_z} e^{-iH_m^{SP}t}, \quad (6)$$

where ω is here designated as the rotating frame frequency. In this frame, the Hamiltonian $H^{SP}(t)$ transforms according to $H(t) = R^{\dagger}(t) H^{SP}(t) R(t) - i\hbar R^{\dagger}(t) \dot{R}(t)$, and can be decomposed as

$$H(t) = H_e + H_{int}(t), \quad (7)$$

where

$$H_e = \frac{\hbar\Delta_e}{2}\sigma_z, \quad (8)$$

with $\Delta_e = \omega_e - \omega$ being the modified electronic frequency, and

$$H_{int}(t) = \sum_{\alpha=x,y} \sum_{l=1}^2 \frac{\hbar\Omega_{\alpha,l}}{2} (\sigma_{ge} e^{-i\omega t} + \sigma_{ge}^{\dagger} e^{i\omega t}) \times \left\{ 1 + i\lambda(a_{\alpha} e^{-i\omega_m t} + a_{\alpha}^{\dagger} e^{i\omega_m t}) e^{-i(\omega_{\alpha,l}^L t - \phi)} + \text{H.c.} \right\}. \quad (9)$$

Furthermore, the ion state in the rotating frame satisfies the master equation

$$\dot{\rho}(t) = \frac{1}{i\hbar} [H(t), \rho(t)] + \sum_{\alpha=x,y} \frac{\kappa}{2} D[a_{\alpha}] \rho(t), \quad (10)$$

where $\rho(t) = R^{\dagger}(t) \rho^{SP}(t) R(t)$. All engine simulations related to the physical model described in this section are performed within this rotating frame.

III. UNITARY STROKE

After introducing the physical model, we proceed to describe the evolution of the two-level system throughout the strokes of the quantum Otto cycle, beginning with the unitary strokes. In these strokes, the electronic component of the ion (ECI) evolves unitarily while its modified frequency changes from an initial value $\Delta_e(0)$ to a final value $\Delta_e(\tau)$ according to a time-dependent function $\Delta_e(t)$. When the modified electronic frequency increases, the unitary stroke is called an expansion stroke; otherwise, it is called a compression stroke.

To induce the change in the modified electronic frequency and ensure that the ECI evolves unitarily, we consider the interaction between the ion and an electric field of a laser beam propagating along the x -direction, with a time-dependent frequency $\omega^L(t) \equiv \omega_{x,1}^L(t) = \omega(t)$. By eliminating the summations in Eq. (9) (setting $\alpha=x$ and $l=1$) and choosing $\phi=0$, the rotating-wave approximation yields the interaction Hamiltonian [46]

$$H_{int} = \frac{\hbar\Omega}{2} (\sigma_{ge} + \sigma_{ge}^{\dagger}), \quad (11)$$

where $\Omega \equiv \Omega_{x,1}$ is the Rabi frequency. Consequently, the dynamics of the electronic state $\rho_e(t) = \text{tr}_m[\rho(t)]$ obeys the von Neumann equation

$$\dot{\rho}_e(t) = \frac{1}{i\hbar} [H_e(t) + H_{int}, \rho_e(t)], \quad (12)$$

with

$$H_e(t) = \frac{\hbar\Delta_e(t)}{2}\sigma_z, \quad (13)$$

where $\Delta_e(t) = \omega_e - \omega^L(t)$. Thus, the ECI evolves from the initial state $\rho_e(0)$ to the final state $\rho_e(\tau) = U_e(\tau)\rho_e(0)U_e^\dagger(\tau)$, in which the unitary evolution operator has the form $U_e(\tau) = T_+ e^{-(i/\hbar)\int_0^\tau dt[H_e(t) + H_{int}]}$, with T_+ being the time-ordering operator.

By examining Eqs. (11) and (13), it is straightforward to see that $[H_e(t) + H_{int}, H_e(t') + H_{int}] \neq 0$ for any t and t' such that $t' \neq t$. This non-commutativity ensures that the unitary stroke described above can induce transitions between the electronic states $|g\rangle$ and $|e\rangle$, depending on the duration of the stroke τ . The transition probability between these electronic states is given by

$$\xi(\tau) = |\langle e | U_e(\tau) | g \rangle|^2. \quad (14)$$

In most cases, transitions between $|g\rangle$ and $|e\rangle$ are undesirable because they are associated with entropy production (irreversibility) [45], which typically reduces engine efficiency. For instance, this applies to the QOHE in which a two-level system operates with two thermal reservoirs [27] and its modified version where the hot thermal reservoir is replaced by a squeezed one [37]. In contrast, transitions during the unitary strokes can be beneficial when the two-level system operates with the hot heat reservoir at an apparent negative temperature, as they may enhance engine efficiency [28]. Therefore, it is interesting to consider scenarios involving such transitions in the unitary stroke described above.

IV. NON-UNITARY STROKE

Now, we proceed to describe the non-unitary strokes, which involve the thermalization process between the ECI and a specified effective heat reservoir. During these strokes, we maintain the electronic frequency constant while allowing the ion to interact, in addition to the dissipation channels for the vibrational modes, with a specific set of laser beams, which gives rise to the desired effective heat reservoir for its electronic component. Below, we describe the procedure to generate effective reservoirs such as (i) an effective thermal reservoir, (ii) an effective heat reservoir with an apparent negative temperature, and (iii) an effective squeezed thermal reservoir. We begin by addressing the effective squeezed thermal reservoir, which makes it easier to approach the remaining effective heat reservoirs.

To generate the effective squeezed thermal reservoir, we assume that the ion interacts with the four laser beams introduced in Sec. II, see Eq. (9). Additionally, we set their frequencies as follows: $\omega_{\alpha,1}^L = \omega - \omega_m$ and $\omega_{\alpha,2}^L = \omega + \omega_m$ ($\alpha = x, y$), where ω is now a short notation for $\omega(0)$ or $\omega(\tau)$ from Sec. III. In this case, restricting to the Lamb-Dicke regime, applying the rotating-

wave approximation, and setting $\phi = -\pi/2$, the interaction Hamiltonian (Eq. (9)) becomes

$$H_{int} = \sum_{\alpha=x,y} \hbar (s_\alpha a_\alpha^\dagger + s_\alpha^\dagger a_\alpha), \quad (15)$$

with

$$s_\alpha = \frac{\lambda}{2} (\Omega_{\alpha,1} \sigma_{ge} + \Omega_{\alpha,2} \sigma_{ge}^\dagger). \quad (16)$$

Then, taking into account Eq. (15) in Eq. (10), assuming $\kappa \gg \lambda \Omega_{\alpha,l}$ so that $\rho(t) \approx \rho_e(t) \otimes |0_x\rangle\langle 0_x| \otimes |0_y\rangle\langle 0_y|$, where $|0_\alpha\rangle$ is the motional ground state in the α direction, and tracing over the motional degrees of freedom, we can employ the adiabatic elimination (as detailed in App. A) [47, 48] to obtain the effective master equation

$$\dot{\rho}_e(t) = \frac{1}{i\hbar} [H_e, \rho_e(t)] + \sum_{\alpha=x,y} \frac{2}{\kappa} D[s_\alpha] \rho_e(t), \quad (17)$$

in which H_e now represents either $H_e(0)$ or $H_e(\tau)$, depending on the stroke considered.

Now that we have Eq. (17) at our disposal, it remains to compare it with the master equation derived by considering a squeezed thermal reservoir to adjust our parameters accordingly. Explicitly, we must compare Eq. (17) with the master equation [49]

$$\dot{\rho}_e(t) = \frac{1}{i\hbar} [H_e, \rho_e(t)] + \sum_{i=1}^2 \frac{1}{2} D[O_i] \rho_e(t), \quad (18)$$

in which

$$O_1 = \sqrt{\gamma(1+n_R)} (\mu \sigma_{ge} + \nu \sigma_{ge}^\dagger), \quad (19)$$

and

$$O_2 = \sqrt{\gamma n_R} (\nu \sigma_{ge} + \mu \sigma_{ge}^\dagger). \quad (20)$$

Here, γ is the electronic decay rate (related to the coupling of the ion to a squeezed thermal reservoir), n_R is the average number of photons in the thermal reservoir before squeezing (which follows from the Bose-Einstein distribution), $\mu = \cosh(r)$, and $\nu = \sinh(r)$, with r being the squeezing parameter. Upon comparing Eq. (17) with Eq. (18), it becomes evident that if we chose

$$\frac{\lambda \Omega_{x,1}}{\sqrt{\kappa}} = \sqrt{\gamma(1+n_R)} \mu, \quad (21)$$

$$\frac{\lambda \Omega_{x,2}}{\sqrt{\kappa}} = \sqrt{\gamma(1+n_R)} \nu, \quad (22)$$

$$\frac{\lambda \Omega_{y,1}}{\sqrt{\kappa}} = \sqrt{\gamma n_R} \nu, \quad (23)$$

and

$$\frac{\lambda \Omega_{y,2}}{\sqrt{\kappa}} = \sqrt{\gamma n_R} \mu, \quad (24)$$

we ensure that Eq. (17) reproduces the dynamics of a two-level system weakly coupled to a squeezed thermal reservoir.

Before proceeding to the remaining effective heat reservoirs, it is worthwhile to show the state that the ECI reaches when equilibrating with the effective squeezed thermal reservoir. By solving Eq. (18) and taking $t \rightarrow \infty$, we obtain the steady-state [49]

$$\rho_e^S = S_{\mu,\nu}(\rho_e^G), \quad (25)$$

in which ρ_e^G is the so-called Gibbs state, and $S_{\mu,\nu}(\cdot)$ is such that

$$S_{\mu,\nu}(|g\rangle\langle g|) = \frac{1}{\mu^2 + \nu^2} (\mu^2 |g\rangle\langle g| + \nu^2 |e\rangle\langle e|), \quad (26)$$

and

$$S_{\mu,\nu}(|e\rangle\langle e|) = \frac{1}{\mu^2 + \nu^2} (\nu^2 |g\rangle\langle g| + \mu^2 |e\rangle\langle e|). \quad (27)$$

The Gibbs state has the form

$$\rho_e^G = \frac{e^{-\beta_R H_e}}{Z_e}, \quad (28)$$

where $\beta_R = 1/(k_B T_R)$, with T_R being the temperature of the effective thermal reservoir before squeezing, and $Z_e = \text{tr}(e^{-\beta_R H_e})$. So, if Eqs. (21)-(24) are satisfied, ρ_e^S is the electronic state after equilibration.

We now address the effective thermal reservoir either at positive or apparent negative temperatures. The procedure we follow here is similar to the one performed above: we compare Eq. (17) with the master equation obtained by considering the desired heat reservoir, aiming to identify the conditions that make these equations identical. The master equation we must compare with Eq. (17) follows the same structure as Eq. (18) but with operators [50, 51]

$$O_1 = \sqrt{\gamma(1 \pm n_R)} \sigma_{ge} \quad (29)$$

and

$$O_2 = \sqrt{\gamma n_R} \sigma_{ge}^\dagger. \quad (30)$$

In Eq. (30), we apply the positive sign if $n_R = 1/(e^{\beta_R \hbar \Delta_e} - 1)$, following the Bose-Einstein distribution ($n_R \in (0, \infty)$), and the negative sign if $n_R = 1/(e^{\beta_R \hbar \Delta_e} + 1)$, following the Fermi-Dirac distribution ($n_R \in (0, 1)$). When n_R corresponds to the Fermi-Dirac distribution and $n_R \in (1/2, 1)$, $\beta_R < 0$; for $n_R \in (0, 1/2)$, $\beta_R > 0$. Therefore, when we consider O_1 and O_2 as defined by Eqs. (29) and (30), Eq. (18) covers both master equations corresponding to a thermal reservoir ($\beta_R > 0$) and a heat reservoir with an apparent negative temperature ($\beta_R < 0$). Then, by comparing this equation with Eq. (17), we obtain

$$\frac{\lambda \Omega_{x,1}}{\sqrt{\kappa}} = \sqrt{\gamma(1 \pm n_R)}, \quad (31)$$

$$\frac{\lambda \Omega_{x,2}}{\sqrt{\kappa}} = 0, \quad (32)$$

$$\frac{\lambda \Omega_{y,1}}{\sqrt{\kappa}} = 0, \quad (33)$$

and

$$\frac{\lambda \Omega_{y,2}}{\sqrt{\kappa}} = \sqrt{\gamma n_R}. \quad (34)$$

Thus, if we configure the laser beams to satisfy Eqs. (31)-(34), Eq. (17) reproduces the dynamics of a two-level system in contact with a thermal reservoir, either at positive or at apparent negative temperatures. As it is well known, under the conditions above the steady-state of Eq. (17) is the Gibbs state displayed in Eq. (28), with $\beta_R > 0$ or $\beta_R < 0$, depending on O_1 and O_2 .

V. QUANTUM OTTO HEAT ENGINE

We begin this section by describing the quantum Otto cycle corresponding to the QOHE we are interested in simulating. As previously mentioned, our goal here is to simulate in the context of trapped ions a QOHE whose working substance is a two-level system operating between a cold and a hot heat reservoir. We assume that the cold heat reservoir is always a thermal reservoir. On the other hand, the hot heat reservoir can be a thermal reservoir, a heat reservoir with an apparent negative temperature, or a squeezed thermal reservoir. As discussed previously, the two-level system corresponds to the ECI, which can effectively interact with these reservoirs. To facilitate the exposition, we initially describe the quantum Otto cycle with an effective squeezed thermal reservoir as its hot heat reservoir. The strokes that constitute the quantum Otto cycle are as follows (see Fig. 1):

Expansion stroke. In this first stroke, the ECI undergoes the unitary evolution described by $U_e^{\text{exp}}(\tau)$, which corresponds to the unitary operator $U_e(\tau)$ introduced in Sec. III, with $\Delta_e(0) = \Delta_e^c$ and $\Delta_e(\tau) = \Delta_e^h$ ($\Delta_e^c < \Delta_e^h$). Here, we consider that Δ_e^c switches to Δ_e^h according to $\Delta_e(t) = (1-t/\tau) \Delta_e^c + (t/\tau) \Delta_e^h$. At the beginning of this stroke, the ECI is in the Gibbs state $\rho_e^{G,c} = e^{-\beta_R^c H_e^c} / Z_e^c$, in which $\beta_R^c = 1/k_B T_R^c$, with T_R^c being the temperature of the effective cold thermal reservoir, $H_e^c = \hbar \Delta_e^c \sigma_z / 2$, and $Z_e^c = \text{tr}(e^{-\beta_R^c H_e^c})$. Note that the superscript “c” denotes that we are referring to the effective cold heat reservoir. Then, the electronic state at the end of the unitary evolution is $\rho_e^{\text{exp}}(\tau) = U_e^{\text{exp}}(\tau) \rho_e^{G,c} U_e^{\text{exp},\dagger}(\tau)$.

Heating stroke. At this stroke, the ECI evolves non-unitarily by interacting effectively with the squeezed hot thermal reservoir, as addressed in Sec. IV. Therefore, the dynamics of the electronic state is governed by Eq. (17), with the parameters meeting the conditions specified in Eqs. (21)-(24). To explicitly indicate that we are

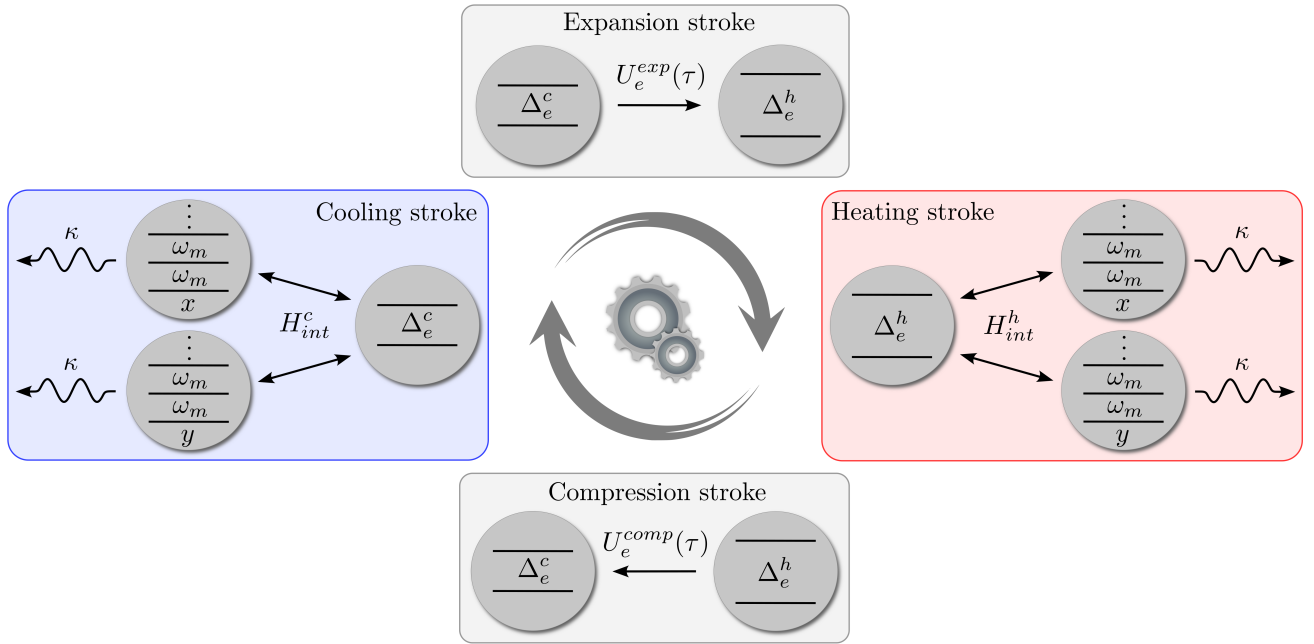


Figure 1. Scheme displaying the quantum Otto cycle described in the text. The boxes represent the cycle strokes. Starting with the cooling stroke, Δ_e^c corresponds to the modified electronic frequency of the ion, ω_m represents the motional frequency of the ion along the x - and y -directions, κ denotes the motional decay rate, and H_{int}^c stands for the interaction Hamiltonian between the electronic and motional components of the ion. As the text explains, H_{int}^c determines the effective cold heat reservoir for the electronic component of the ion (ECI). In the expansion stroke, the two-level system undergoes a unitary evolution governed by $U_e^{exp}(\tau)$, which changes the modified electronic frequency from Δ_e^c to Δ_e^h ($\Delta_e^c < \Delta_e^h$) after time τ . During the heating stroke, the interaction Hamiltonian is now H_{int}^h , which leads to the effective hot heat reservoir for the ECI. Finally, in the compression stroke, the unitary operator $U_e^{comp}(\tau)$ reverses the change, bringing the modified electronic frequency back from Δ_e^h to Δ_e^c .

dealing with the effective hot heat reservoir, we use the superscript “ h ” in these equations, resulting in the notation changes $H_e \rightarrow H_e^h = \hbar \Delta_e^h \sigma_z / 2$, $s_\alpha \rightarrow s_\alpha^h = \lambda (\Omega_{\alpha,1}^h \sigma_- + \Omega_{\alpha,2}^h \sigma_+)/2$, and $n_R \rightarrow n_R^h$. The stroke ends when the ECI equilibrates with the effective hot heat reservoir, reaching the steady-state $\rho_e^{S,h} = S_{\mu,\nu}(\rho_e^{G,h})$, where $\rho_e^{G,h} = e^{-\beta_R^h H_e^h} / Z_e^h$. Here, $\beta_R^h = 1/k_B T_R^h$, with T_R^h being the temperature of the hot thermal reservoir before squeezing, and $Z_e^h = \text{tr}(e^{-\beta_R^h H_e^h})$.

Compression stroke. During this stroke, the electronic state evolves unitarily according to $U_e^{comp}(\tau) = U_e^{exp,\dagger}(\tau)$, which matches the adjoint of $U_e(\tau)$ from Sec. III, observing that now $\Delta_e(0) = \Delta_e^h$ and $\Delta_e(\tau) = \Delta_e^c$ (here, $\Delta_e(t) = (1-t/\tau) \Delta_e^h + (t/\tau) \Delta_e^c$). As a result, the present stroke leads the ECI to the state $\rho_e^{comp}(\tau) = U_e^{comp}(\tau) \rho_e^{S,h} U_e^{comp,\dagger}(\tau)$.

Cooling stroke. As a final stroke, the ECI interacts effectively with the cold thermal reservoir until thermalization. Here, as discussed in Sec. IV, the electronic state undergoes a non-unitary evolution dictated by Eq. (17), obeying Eqs. (31)-(34). To explicitly denote that we are referring to the effective cold heat reservoir, we introduce the superscript “ c ” in these equations, leading to the notation modifications $H_e \rightarrow H_e^c$,

$s_\alpha \rightarrow s_\alpha^c = \lambda (\Omega_{\alpha,1}^c \sigma_- + \Omega_{\alpha,2}^c \sigma_+)/2$, and $n_R \rightarrow n_R^c$. When the thermalization occurs, the ECI reaches the Gibbs state $\rho_e^{G,c}$, thus closing the cycle.

After describing the cycle, we can proceed to determine the engine efficiency. For this purpose, we first calculate the heat and work associated with each cycle stroke. To obtain these quantities, we adopt the following definitions for work and heat [52, 53]: $W_e^{str} = \int_{t_i}^{t_f} dt \text{tr}[\dot{H}_e^{str}(t) \rho_e^{str}(t)]$ and $Q_e^{str} = \int_{t_i}^{t_f} dt \text{tr}[H_e^{str}(t) \dot{\rho}_e^{str}(t)]$. Here, $H_e^{str}(t)$ and $\rho_e^{str}(t)$ correspond to the Hamiltonian and the state that describe the ECI throughout the respective strokes. With these definitions, it is straightforward to show that the expansion and compression strokes involve only work (W_e^{comp} and W_e^{exp}), whereas the heating and cooling strokes involve solely heat (Q_e^h and Q_e^c). Thus, by calculating the energy exchanged in each stroke, we obtain the net work ($W_e^{net} = W_e^{exp} + W_e^{comp}$)

$$W_e^{net} = -\frac{\hbar(\Delta_e^h - \Delta_e^c)}{2} [\tanh(\theta^c) - \zeta \tanh(\theta^h)] + \hbar \xi [\Delta_e^h \tanh(\theta^c) + \Delta_e^c \zeta \tanh(\theta^h)], \quad (35)$$

the heat associated with the heating stroke

$$Q_e^h = \frac{\hbar \Delta_e^h}{2} [\tanh(\theta^c) - \zeta \tanh(\theta^h) - 2\xi \tanh(\theta^c)], \quad (36)$$

and the heat linked to the cooling stroke

$$Q_e^c = -\frac{\hbar\Delta_e^c}{2} [\tanh(\theta^c) - \zeta \tanh(\theta^h) + 2\xi \zeta \tanh(\theta^h)], \quad (37)$$

where $\theta^{c(h)} = \beta_R^{c(h)} \hbar \Delta_e^{c(h)} / 2$ and $\zeta = 1/(\mu^2 + \nu^2)$, as derived in Ref. [37]. For the sake of simplicity, we are omitting the time dependence of the probability transition ($\xi \equiv \xi(\tau)$).

The condition for the cycle presented above to operate as a heat engine is $W_e^{net} < 0$, indicating the extraction of net work from the ECI after the four strokes. If this condition is satisfied, the engine efficiency η is determined using the formula

$$\eta = -\frac{W_e^{net}}{Q_e^{abs}}, \quad (38)$$

with Q_e^{abs} representing the heat absorbed by the ECI ($Q_e^{abs} > 0$) during the cycle. Considering Eqs. (35)-(37), it is easy to demonstrate that $W_e^{net} < 0$ implies $Q_e^h > 0$ and $Q_e^c < 0$, resulting in $Q_e^{abs} = Q_e^h$. As a result, the engine efficiency can be expressed as [37]

$$\eta^S = 1 - \frac{\Delta_e^c}{\Delta_e^h} \left[\frac{\tanh(\theta^c) - (1-2\xi)\zeta \tanh(\theta^h)}{(1-2\xi)\tanh(\theta^c) - \zeta \tanh(\theta^h)} \right]. \quad (39)$$

As stated in Ref. [37], η^S cannot surpass the Otto efficiency $\eta_O = 1 - \Delta_e^c / \Delta_e^h$ but can exceed the Carnot efficiency $\eta_C = 1 - \beta_R^h / \beta_R^c$. This is because the squeezing process actually adds photons into the hot heat reservoir, increasing its effective temperature when compared to its initial temperature T_R^h .

We can now easily adjust the cycle and expressions introduced above to account for the cases where the QOHE operates with a thermal reservoir and a heat reservoir with an apparent negative temperature as its hot heat reservoir. The adjustment in the cycle involves allowing the ECI to interact effectively with one of these heat reservoirs, which changes the final electronic state of the heating stroke and, consequently, the initial and final electronic states of the compression stroke. Thus, the ECI attains a Gibbs state (Eq. (28)) at the end of the heating stroke, with $\beta_R^h > 0$ for the effective hot thermal reservoir and $\beta_R^h < 0$ for the effective hot heat reservoir with an apparent negative temperature. Subsequently, we obtain the final electronic state of the compression stroke by applying $U_e^{comp}(\tau)$ to the respective Gibbs state. As a result, we can rewrite Eqs. (35)-(37) by taking $r=0$ (which implies $S_{\mu,\nu}(\cdot) = I$ and $\zeta = 1$) and, if we are considering an effective hot heat reservoir with an apparent negative temperature, $\beta_R^h = -|\beta_R^h|$ ($\theta^h = -|\theta^h|$). In the case involving an effective hot thermal reservoir, $W_e^{net} < 0$ then results in $Q_e^h > 0$ and $Q_e^c < 0$ ($Q_e^{abs} = Q_e^h$), allowing us to express the engine efficiency as [27]

$$\eta^+ = 1 - \frac{\Delta_e^c}{\Delta_e^h} \left[\frac{\tanh(\theta^c) - (1-2\xi)\tanh(\theta^h)}{(1-2\xi)\tanh(\theta^c) - \tanh(\theta^h)} \right]. \quad (40)$$

On the other hand, in the case involving an effective hot heat reservoir with an apparent negative temperature, $W_e^{net} < 0$ does not always imply $Q_e^h > 0$ and $Q_e^c < 0$; there are values of ξ that yield $Q_e^h > 0$ and $Q_e^c > 0$. If the ECI absorbs heat from both effective heat reservoirs, $\eta^- = 1$, whereas if it absorbs heat only from the effective hot heat reservoir [28],

$$\eta^- = 1 - \frac{\Delta_e^c}{\Delta_e^h} \left[\frac{\tanh(\theta^c) + (1-2\xi)\tanh(|\theta^h|)}{(1-2\xi)\tanh(\theta^c) + \tanh(|\theta^h|)} \right]. \quad (41)$$

As discussed in Ref. [28], the hot heat reservoir with an apparent negative temperature can lead to $\eta^- > \eta_O$, depending on the value of ξ .

VI. NUMERICAL RESULTS

In this section, we present some numerical results that illustrate the effectiveness of the proposed scheme in simulating the QOHE of interest. For this purpose, we numerically replicate the cycles described in the previous section, considering both the scenario in which we perform the adiabatic elimination (in the heating and cooling strokes) and the one where we do not. By applying this approximation, we obtain the dynamics of the ECI utilizing Eq. (17); otherwise, we use Eq. (10) with the interaction Hamiltonian provided by Eq. (15). In this way, we can verify the accuracy of the adiabatic elimination, which gives rise to the desired effective dynamics during the heating and cooling strokes. Furthermore, while ensuring the Lamb-Dicke regime and the validity of the rotating wave approximation, we select parameters of the same order as those observed in experimental setups involving trapped ions [46, 54, 55]. We obtain the numerical results using the Quantum Toolbox in Python (QuTiP) [56, 57].

The numerical results are shown in Figs. 2(a)-(c), where we display the engine efficiency η as a function of the transition probability ξ . Fig. 2(a) corresponds to the case involving an effective hot thermal reservoir (η^+), Fig. 2(b) to the situation involving an effective hot heat reservoir with an apparent negative temperature (η^-), and Fig. 2(c) to the scenario involving an effective squeezed hot thermal reservoir (η^S). In these figures, we set $\Delta_e^c = 2\pi \times (0.2 \text{ MHz})$, $\Delta_e^h = 2\pi \times (0.4 \text{ MHz})$, $\lambda = 10^{-2}$, $\Omega = 2\pi \times (10 \text{ MHz})$, $\kappa = 2\pi \times (1 \text{ MHz})$, $\gamma = 2\pi \times (10^{-3} \text{ MHz})$, and $n_R^c = 0.6$ (given by the Bose-Einstein distribution). Additionally, we assume $n_R^h = 1.2$ (provided by the Bose-Einstein distribution) in Fig. 2(a), $n_R^h = 0.8$ (given by the Fermi-Dirac distribution) in Fig. 2(b), and $n_R^h = 0.4$ (determined by the Bose-Einstein distribution) and $r = 1.5$ in Fig. 2(c). With these quantities, it is straightforward to calculate the respective Rabi frequencies $\Omega_{x,1}^{c(h)}$, $\Omega_{x,2}^{c(h)}$, $\Omega_{y,1}^{c(h)}$, and $\Omega_{y,2}^{c(h)}$ by using Eqs. (21)-(24) or (31)-(34), depending on the case. Therefore, since the parameters are adjusted to reproduce the desired dynamics, it remains solely to verify the validity

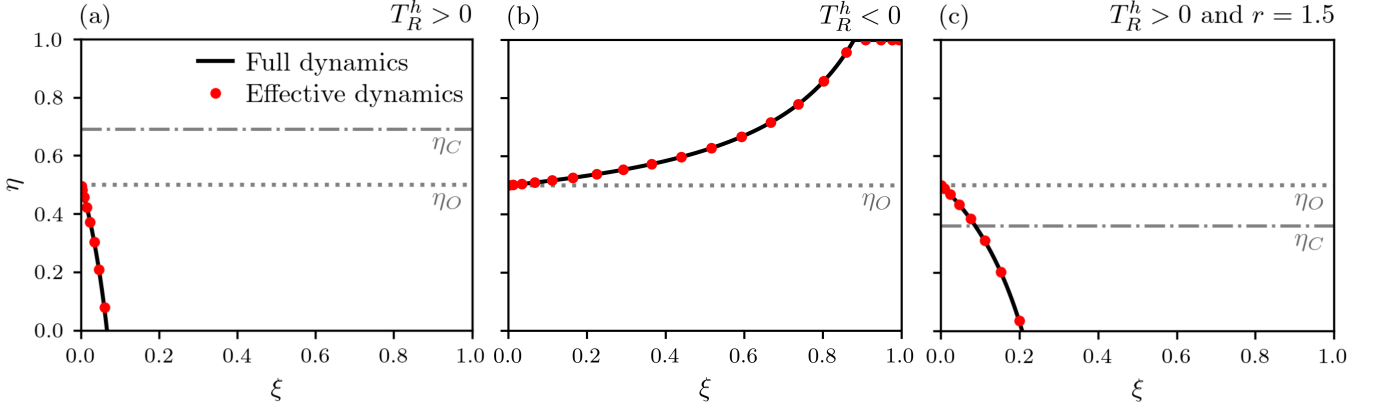


Figure 2. Engine efficiency η as a function of the transition probability ξ . Panel (a) displays curves associated with the effective hot thermal reservoir, panel (b) shows curves related to the effective hot reservoir with an apparent negative temperature, and panel (c) depicts curves linked with the effective hot squeezed thermal reservoir. In panels (a)-(c), we assume a cold thermal reservoir with $n_R^c=0.6$, defined by the Bose-Einstein distribution. In panel (a), we choose $n_R^h=1.2$, determined by the Bose-Einstein distribution; in panel (b), $n_R^h=0.8$, given by the Fermi-Dirac distribution; and in panel (c), $n_R^h=0.4$, provided by the Bose-Einstein distribution, and $r=1.5$. In addition, we set $\Delta_e^c=2\pi\times(0.2\text{ MHz})$, $\Delta_e^h=2\pi\times(0.4\text{ MHz})$, $\lambda=10^{-2}$, $\Omega=2\pi\times(10\text{ MHz})$, $\kappa=2\pi\times(1\text{ MHz})$, and $\gamma=2\pi\times(10^{-3}\text{ MHz})$. The red dots correspond to the case in which we apply the adiabatic elimination in the heating and cooling strokes (effective dynamics), the black solid lines correspond to the situation in which we do not perform the adiabatic elimination (full dynamics), the gray dotted lines show the Otto efficiency η_O , and the gray dot-dashed lines display the Carnot efficiency η_C .

of the approximations employed to obtain the effective dynamics. In Figs. 2(a)-(c), the red dots correspond to the case in which we perform the adiabatic elimination (effective dynamics), derived in detail in App. A, while the solid black lines are associated with the scenario in which we do not perform such an approximation (full dynamics). Besides, the gray dotted and dot-dashed lines indicate the corresponding Otto and Carnot efficiencies, respectively. As we can see, the red dots overlap the black solid ones, thus illustrating the validity of the adiabatic elimination applied to derive Eq. (18).

VII. HOW ABOUT A QUANTUM HARMONIC OSCILLATOR AS THE WORKING SUBSTANCE?

Having addressed the case involving a two-level system as the working substance, we now briefly discuss the simulation of a QOHE that has a quantum harmonic oscillator as the working substance. To simulate such a QOHE, considering the different types of heat reservoirs discussed previously, we need a physical model different from the one presented in Sec. II. Here, considering only the oscillation of the ion in a given direction, assuming that three energy levels in the V configuration define its electronic structure, and allowing it to interact with a set of four laser beams (as in Sec. II), the Hamiltonian that describes the ion is

$$H^{SP}(t)=H_e^{SP}+H_m^{SP}+H^{SP}(t), \quad (42)$$

with

$$H_e^{SP}=\frac{\hbar\omega_{ge}}{2}|e\rangle\langle e|+\frac{\hbar\omega_{gf}}{2}|f\rangle\langle f|, \quad (43)$$

$$H_m^{SP}=\hbar\omega_ma^\dagger a, \quad (44)$$

and (in the Lamb-Dicke regime)

$$H_{int}^{SP}(t)=\sum_{\alpha=ge,gf}\sum_{l=1}^2\frac{\hbar\Omega_{\alpha,l}}{2}(\sigma_\alpha+\sigma_\alpha^\dagger)\times\left\{1+i\lambda(a+a^\dagger)e^{-i(\omega_{\alpha,l}^L t-\phi)}+\text{H.c.}\right\}. \quad (45)$$

In Eq. (43), $|e\rangle$ and $|f\rangle$ are the excited electronic states, while ω_{ge} and ω_{gf} are the electronic transition frequencies between them and the ground state $|g\rangle$; in Eq. (45), $\sigma_{gf}=|g\rangle\langle f|$ ($\sigma_{gf}^\dagger=|f\rangle\langle g|$). Furthermore, we assume that the dynamics of the ion state is given now by the master equation

$$\dot{\rho}^{SP}(t)=\frac{1}{i\hbar}[H^{SP}(t),\rho^{SP}(t)]+\sum_{\alpha=ge,gf}\frac{\gamma_\alpha}{2}D[\sigma_\alpha]\rho^{SP}(t), \quad (46)$$

where γ_{ge} and γ_{gf} are the electronic decay rates. Here, in contrast to Sec. II, we consider the motional decay rate to be significantly smaller than the electronic decay rates, which can be achieved, for instance, by working with motional modes that inherently possess long coherence times. Consequently, we can safely disregard it.

Now, similarly to Sec. II, we switch to the rotating frame defined by the unitary transformation

$$R(t)=e^{-iH_e^{SP}t}e^{-i(\omega t)a^\dagger a}, \quad (47)$$

resulting in the master equation

$$\dot{\rho}(t)=\frac{1}{i\hbar}[H(t),\rho(t)]+\sum_{\alpha=ge,gf}\frac{\gamma_\alpha}{2}D[\sigma_\alpha]\rho(t), \quad (48)$$

in which

$$H(t) = H_m + H_{int}(t), \quad (49)$$

with

$$H_m = \hbar \Delta_m a^\dagger a, \quad (50)$$

being $\Delta_m = \omega_m - \omega$, and

$$H_{int}(t) = \sum_{\alpha=ge, gf} \sum_{l=1}^2 \frac{\hbar \Omega_{\alpha,l}}{2} (\sigma_\alpha e^{-i\omega_\alpha t} + \sigma_\alpha^\dagger e^{i\omega_\alpha t}) \times \times \left\{ 1 + i\lambda (a e^{-i\omega t} + a^\dagger e^{i\omega t}) e^{-i(\omega_{\alpha,l}^L t - \phi)} + \text{H.c.} \right\}. \quad (51)$$

Having defined the physical model, we can now describe the generation of the effective heat reservoirs of interest for the quantum harmonic oscillator. Following the same strategy as in Sec. IV, we start by setting $\omega_{\alpha,1}^L = \omega - \omega_\alpha$, $\omega_{\alpha,2}^L = \omega + \omega_\alpha$, and $\phi = -\pi/2$. As a result, the rotating-wave approximation lead to the interaction Hamiltonian

$$H_{int} = \sum_{\alpha=ge, gf} \hbar (s_\alpha \sigma_\alpha^\dagger + s_\alpha^\dagger \sigma_\alpha), \quad (52)$$

in which

$$s_\alpha = \frac{\lambda}{2} (\Omega_{\alpha,1} a + \Omega_{\alpha,2} a^\dagger). \quad (53)$$

Then, assuming $\gamma_\alpha \gg \lambda \Omega_{\alpha,l}$ so that $\rho(t) \approx |g\rangle \langle g| \otimes \rho_m(t)$, tracing over the electronic degree of freedom, and applying the adiabatic elimination (see App. B), we obtain the effective master equation

$$\dot{\rho}_m(t) = \frac{1}{i\hbar} [H_m, \rho_m(t)] + \sum_{\alpha=ge, gf} \frac{2}{\gamma_\alpha} D[s_\alpha] \rho_m(t). \quad (54)$$

Thus, when we properly choose the Rabi frequencies, obeying similar relations to the ones of Eqs. (21)-(24) and (31)-(34), Eq. (54) can effectively describe the dynamics of the quantum harmonic oscillator in contact with the heat reservoirs discussed in the previous sections.

Finally, we implement the unitary steps of the cycle by turning off the laser beams and modifying the trap potential, which changes ω_m and, consequently, Δ_m . Note that variations in ω_m can induce transitions in the motional part of the ion, since $[H_m(t), H_m(t')] \neq 0$ for any t and t' such that $t' \neq t$.

VIII. CONCLUSION

We present a scheme that utilizes an ion confined within a bi-dimensional trap to simulate a quantum Otto

heat engine (QOHE) with a two-level system as its working substance. Our scheme allows the electronic component of the ion (ECI), here considered as a two-level system, to interact with different types of effective heat reservoirs, including effective thermal reservoirs (effective heat reservoirs with positive temperatures), effective heat reservoirs with apparent negative temperatures, and effective squeezed thermal reservoirs. We describe how to generate these effective heat reservoirs and detail the strokes of the quantum Otto cycle. For comparison purposes, we display the efficiency of the QOHE when the ECI operates under three scenarios: (i) with two effective thermal reservoirs, (ii) with an effective thermal reservoir and an effective heat reservoir with a negative apparent temperature, and (iii) with an effective thermal reservoir and an effective squeezed thermal reservoir. For all scenarios, we present numerical results that illustrate the applicability of our scheme by comparing the engine efficiencies obtained from the physical models with and without the adiabatic elimination, which is the primary approximation for generating the effective heat reservoirs mentioned above. Beyond the parameter regime of this approximation, correlations between the electronic and motional components of the ion can become significant, complicating the application of the definitions of heat and work employed in this study. Nevertheless, if one is interested in exploring such correlations and other types of reservoirs, the proposed scheme could, in principle, still be applied. Lastly, we also show how to simulate a QOHE whose working substance is a quantum harmonic oscillator operating with the effective heat reservoirs cited above.

ACKNOWLEDGMENTS

We acknowledge financial support from the following Brazilian agencies: Coordenação de Aperfeiçoamento de Pessoal de Nível Superior (CAPES), Financial code 001; National Council for Scientific and Technological Development (CNPq), Grants No. 311612/2021-0 and 301500/2018-5; São Paulo Research Foundation (FAPESP), Grants No. 2019/11999-5, No. 2021/04672-0, and No. 2022/10218-2; and Goiás State Research Support Foundation (FAPEG). This work was performed as part of the Brazilian National Institute of Science and Technology for Quantum Information (INCT-IQ/CNPq), Grant No. 465469/2014-0.

Appendix A: Effective dynamics of the two-level system

In this first appendix, we derive the effective master equation presented in Eq. (17) of the main text. To achieve this, we utilize the projection-based adiabatic elimination method described in Refs. [47, 48] to eliminate the fast degrees of freedom of the ion.

We begin by writing the Liouvillian superoperator for the ion, considering the operator-vector isomorphism defined by the map $|\psi_e\rangle\langle\psi'_e|\otimes|\psi_x\rangle\langle\psi'_x|\otimes|\psi_y\rangle\langle\psi'_y|\mapsto|\psi_e\rangle\otimes|\psi_e\rangle^*\otimes|\psi_x\rangle\otimes|\psi_x\rangle^*\otimes|\psi_y\rangle\otimes|\psi_y\rangle^*$. Thus, the master equation for the ion is mapped into the equation $|\dot{\rho}(t)\rangle=\mathcal{L}|\rho(t)\rangle$, where $|\rho(t)\rangle$ is the vectorized density operator and \mathcal{L} is the Liouvillian superoperator acting on the vector space in which $|\rho(t)\rangle$ is defined. By making the tensor products explicit, Eq. (10) (with H_{int} given by Eq. (15)) provides the Liouvillian superoperator

$$\mathcal{L}=\mathcal{L}_e\otimes I_{2m}+I_{2e}\otimes\mathcal{L}_m+\mathcal{L}_{int}, \quad (\text{A1})$$

where

$$\mathcal{L}_e=-\frac{i\Delta_e}{2}(\sigma_z\otimes I_e-I_e\otimes\sigma_z), \quad (\text{A2})$$

$$I_{2m}=I_x\otimes I_x\otimes I_y\otimes I_y, \quad (\text{A3})$$

$$I_{2e}=I_e\otimes I_e, \quad (\text{A4})$$

$$\mathcal{L}_m=\frac{\kappa}{2}(2a_x\otimes a_x\otimes I_{2y}-a_x^\dagger a_x\otimes I_x\otimes I_{2y}-I_x\otimes a_x^\dagger a_x\otimes I_{2y}+2I_{2x}\otimes a_y\otimes a_y-I_{2x}\otimes a_y^\dagger a_y\otimes I_y-I_{2x}\otimes I_y\otimes a_y^\dagger a_y), \quad (\text{A5})$$

and

$$\begin{aligned} \mathcal{L}_{int}=&-i(s_x\otimes I_e\otimes a_x^\dagger\otimes I_x\otimes I_{2y}+s_x^\dagger\otimes I_e\otimes a_x\otimes I_x\otimes I_{2y}-I_e\otimes s_x\otimes I_x\otimes a_x^\dagger\otimes I_{2y}-I_e\otimes s_x^\dagger\otimes I_x\otimes a_x\otimes I_{2y}) \\ &-i(s_y\otimes I_e\otimes I_{2x}\otimes a_y^\dagger\otimes I_y+s_y^\dagger\otimes I_e\otimes I_{2x}\otimes a_y\otimes I_y-I_e\otimes s_y\otimes I_{2x}\otimes I_y\otimes a_y^\dagger-I_e\otimes s_y^\dagger\otimes I_{2x}\otimes I_y\otimes a_y). \end{aligned} \quad (\text{A6})$$

Here, I_e and $I_x\otimes I_y$ are the identity operators of the electronic and motional parts of the ion, respectively.

As described in Sec. IV, we require that $\kappa\gg\lambda\Omega_{\alpha,i}$ ($\alpha=x,y$ and $i=1,2$), which ensures that the motional component of the ion (MCI) quickly reaches the steady state $|\rho_m^{ss}\rangle=|0_x\rangle\otimes|0_x\rangle\otimes|0_y\rangle\otimes|0_y\rangle$. In this regime, the motional dynamics approximately occur within the subspace spanned by the basis presented in Tab. I. Thus, the slow dynamics of the MCI takes place in the subspace described by basis $\{|\psi_0\rangle=|\rho_m^{ss}\rangle\}$, while the fast dynamics of the MCI (which we aim to eliminate) occurs in the subspace generated by basis $\{|\psi_1\rangle,|\psi_2\rangle,\dots,|\psi_{15}\rangle\}$.

$ \psi_0\rangle= 0_x\rangle\otimes 0_x\rangle\otimes 0_y\rangle\otimes 0_y\rangle$	$ \psi_1\rangle= 0_x\rangle\otimes 0_x\rangle\otimes 1_y\rangle\otimes 0_y\rangle$	$ \psi_2\rangle= 0_x\rangle\otimes 0_x\rangle\otimes 0_y\rangle\otimes 1_y\rangle$	$ \psi_3\rangle= 0_x\rangle\otimes 0_x\rangle\otimes 1_y\rangle\otimes 1_y\rangle$
$ \psi_4\rangle= 1_x\rangle\otimes 0_x\rangle\otimes 0_y\rangle\otimes 0_y\rangle$	$ \psi_5\rangle= 1_x\rangle\otimes 0_x\rangle\otimes 1_y\rangle\otimes 0_y\rangle$	$ \psi_6\rangle= 1_x\rangle\otimes 0_x\rangle\otimes 0_y\rangle\otimes 1_y\rangle$	$ \psi_7\rangle= 1_x\rangle\otimes 0_x\rangle\otimes 1_y\rangle\otimes 1_y\rangle$
$ \psi_8\rangle= 0_x\rangle\otimes 1_x\rangle\otimes 0_y\rangle\otimes 0_y\rangle$	$ \psi_9\rangle= 0_x\rangle\otimes 1_x\rangle\otimes 1_y\rangle\otimes 0_y\rangle$	$ \psi_{10}\rangle= 0_x\rangle\otimes 1_x\rangle\otimes 0_y\rangle\otimes 1_y\rangle$	$ \psi_{11}\rangle= 0_x\rangle\otimes 1_x\rangle\otimes 1_y\rangle\otimes 1_y\rangle$
$ \psi_{12}\rangle= 1_x\rangle\otimes 1_x\rangle\otimes 0_y\rangle\otimes 0_y\rangle$	$ \psi_{13}\rangle= 1_x\rangle\otimes 1_x\rangle\otimes 1_y\rangle\otimes 0_y\rangle$	$ \psi_{14}\rangle= 1_x\rangle\otimes 1_x\rangle\otimes 0_y\rangle\otimes 1_y\rangle$	$ \psi_{15}\rangle= 1_x\rangle\otimes 1_x\rangle\otimes 1_y\rangle\otimes 1_y\rangle$

Table I. Truncated basis employed to describe the motional component of the ion.

Following the projection-based adiabatic elimination method presented in Refs. [47, 48], the effective Liouvillian superoperator of the ion is given by (see Eq. (19) of Ref. [48])

$$\mathcal{L}_{eff}=\mathcal{L}_e\otimes\mathcal{P}_m+\mathcal{P}\mathcal{L}_{int}\mathcal{P}-\mathcal{P}\mathcal{L}_{int}\mathcal{Q}\left[I_{2e}\otimes(\mathcal{Q}_m\mathcal{L}_m\mathcal{Q}_m)^{-1}\right](I_{2e}\otimes\mathcal{Q}_m\mathcal{L}_m\mathcal{P}_m+\mathcal{Q}\mathcal{L}_{int}\mathcal{P}), \quad (\text{A7})$$

in which $\mathcal{P}=I_{2e}\otimes\mathcal{P}_m$ and $\mathcal{Q}=I_{2e}\otimes\mathcal{Q}_m$, with $\mathcal{P}_m=|\rho_m^{ss}\rangle\langle I_m|$ ($I_m=I_x\otimes I_y$) and $\mathcal{Q}_m=I_{2m}-\mathcal{P}_m$. Note that the projector \mathcal{P} projects the ion dynamics onto the slow subspace, since $\mathcal{P}|\rho(t)\rangle=|\rho_e(t)\rangle\otimes|\rho_m^{ss}\rangle$, while the projector \mathcal{Q} projects the ion dynamics onto the fast subspace. By taking into account Eqs. (A2), (A5) and (A6), we have that

$$\mathcal{P}\mathcal{L}_{int}\mathcal{P}=0, \quad (\text{A8})$$

$$\mathcal{P}\mathcal{L}_{int}\mathcal{Q} = -i[(s_x^\dagger \otimes I_e - I_e \otimes s_x) \otimes |\rho_m^{ss}\rangle \langle \langle \psi_4| + \langle \langle \psi_7| + (s_x \otimes I_e - I_e \otimes s_x^\dagger) \otimes |\rho_m^{ss}\rangle \langle \langle \psi_8| + \langle \langle \psi_{11}| + (s_y^\dagger \otimes I_e - I_e \otimes s_y) \otimes |\rho_m^{ss}\rangle \langle \langle \psi_1| + \langle \langle \psi_{13}| + (s_y \otimes I_e - I_e \otimes s_y^\dagger) \otimes |\rho_m^{ss}\rangle \langle \langle \psi_2| + \langle \langle \psi_{14}|], \quad (\text{A9})$$

$$\mathcal{Q}_m \mathcal{L}_m \mathcal{P}_m = 0, \quad (\text{A10})$$

and

$$\mathcal{Q}\mathcal{L}_{int}\mathcal{P} = -i(s_x \otimes I_e \otimes |\psi_4\rangle \langle \langle I_m| - I_e \otimes s_x \otimes |\psi_8\rangle \langle \langle I_m| + s_y \otimes I_e \otimes |\psi_1\rangle \langle \langle I_m| - I_e \otimes s_y \otimes |\psi_2\rangle \langle \langle I_m|). \quad (\text{A11})$$

Furthermore, with the help of Sympy, we have

$$\begin{aligned} (\mathcal{Q}_m \mathcal{L}_m \mathcal{Q}_m)^{-1} = & -\frac{1}{\kappa}(2|\psi_1\rangle \langle \langle \psi_1| + 2|\psi_2\rangle \langle \langle \psi_2| + |\psi_3\rangle \langle \langle \psi_3| + 2|\psi_4\rangle \langle \langle \psi_4| + |\psi_5\rangle \langle \langle \psi_5| \\ & + |\psi_6\rangle \langle \langle \psi_6| + \frac{2}{3}|\psi_7\rangle \langle \langle \psi_7| + 2|\psi_8\rangle \langle \langle \psi_8| + |\psi_9\rangle \langle \langle \psi_9| + |\psi_{10}\rangle \langle \langle \psi_{10}| + \frac{2}{3}|\psi_{11}\rangle \langle \langle \psi_{11}| \\ & + |\psi_{12}\rangle \langle \langle \psi_{12}| + \frac{2}{3}|\psi_{13}\rangle \langle \langle \psi_{13}| + \frac{2}{3}|\psi_{14}\rangle \langle \langle \psi_{14}| + \frac{1}{2}|\psi_{15}\rangle \langle \langle \psi_{15}| + \frac{4}{3}|\psi_4\rangle \langle \langle \psi_7| \\ & + \frac{4}{3}|\psi_8\rangle \langle \langle \psi_{11}| + \frac{1}{2}|\psi_{12}\rangle \langle \langle \psi_{15}| + \frac{4}{3}|\psi_1\rangle \langle \langle \psi_{13}| + \frac{4}{3}|\psi_2\rangle \langle \langle \psi_{14}| + \frac{1}{2}|\psi_3\rangle \langle \langle \psi_{15}| \end{aligned} \quad (\text{A12})$$

Finally, substituting Eq. (A8)-(A12) into Eq. (A7), we obtain

$$\mathcal{L}_{eff} = \left[\mathcal{L}_e + \sum_{\alpha=x,y} \frac{2}{\kappa} (2s_\alpha \otimes s_\alpha - s_\alpha^\dagger s_\alpha \otimes I_e - I_e \otimes s_\alpha^\dagger s_\alpha) \right] \otimes \mathcal{P}_m, \quad (\text{A13})$$

which leads to Eq. (17).

Appendix B: Effective dynamics of the quantum harmonic oscillator

Here, in this second appendix, we obtain the effective master equation for the motional state shown in Eq. (54) of the main text. As in the first appendix, here we also follow the projection-based adiabatic elimination method introduced in Refs. [47, 48].

Considering the operator-vector isomorphism mentioned in the previous appendix, Eq. (48) (with H_{int} defined by Eq. (52)) leads to the Liouvillian superoperator

$$\mathcal{L} = \mathcal{L}_e \otimes I_{2m} + I_{2e} \otimes \mathcal{L}_m + \mathcal{L}_{int}, \quad (\text{B1})$$

where

$$\mathcal{L}_e = \frac{\gamma_{ge}}{2} (2\sigma_{ge} \otimes \sigma_{ge} - \sigma_{ge}^\dagger \sigma_{ge} \otimes I_e - I_e \otimes \sigma_{ge}^\dagger \sigma_{ge}) + \frac{\gamma_{gf}}{2} (2\sigma_{gf} \otimes \sigma_{gf} - \sigma_{gf}^\dagger \sigma_{gf} \otimes I_e - I_e \otimes \sigma_{gf}^\dagger \sigma_{gf}), \quad (\text{B2})$$

$$I_{2m} = I_m \otimes I_m, \quad (\text{B3})$$

$$\mathcal{L}_m = -i\Delta_m (a^\dagger a \otimes I_m - I_m \otimes a^\dagger a), \quad (\text{B4})$$

and

$$\begin{aligned} \mathcal{L}_{int} = & -i(\sigma_{ge} \otimes I_e \otimes s_{ge}^\dagger \otimes I_m + \sigma_{ge}^\dagger \otimes I_e \otimes s_{ge} \otimes I_m - I_e \otimes \sigma_{ge} \otimes I_m \otimes s_{ge}^\dagger - I_e \otimes \sigma_{ge}^\dagger \otimes I_m \otimes s_{ge}) \\ & - i(\sigma_{gf} \otimes I_e \otimes s_{gf}^\dagger \otimes I_m + \sigma_{gf}^\dagger \otimes I_e \otimes s_{gf} \otimes I_m - I_e \otimes \sigma_{gf} \otimes I_m \otimes s_{gf}^\dagger - I_e \otimes \sigma_{gf}^\dagger \otimes I_m \otimes s_{gf}). \end{aligned} \quad (\text{B5})$$

As stated in Sec. (VII), we assume that $\gamma_\alpha \gg \lambda\Omega_{\alpha,i}$ ($\alpha = ge, gf$ and $i = 1, 2$), which implies that the ECI rapidly reaches the steady state $|\rho_e^{ss}\rangle = |g\rangle \otimes |g\rangle$. With this, the slow and fast subspaces of the ECI is spanned by the basis $\{|\rho_e^{ss}\rangle = |g\rangle \otimes |g\rangle\}$ and $\{|g\rangle \otimes |e\rangle, |g\rangle \otimes |f\rangle, |e\rangle \otimes |g\rangle, |e\rangle \otimes |e\rangle, |e\rangle \otimes |f\rangle, |f\rangle \otimes |g\rangle, |f\rangle \otimes |e\rangle, |f\rangle \otimes |f\rangle\}$, respectively.

According to Ref. [48], the effective Liouvillian superoperator for the ion has the form

$$\mathcal{L}_{eff} = \mathcal{P}_e \otimes \mathcal{L}_m + \mathcal{P} \mathcal{L}_{int} \mathcal{P} - \mathcal{P} \mathcal{L}_{int} \mathcal{Q} \left[(\mathcal{Q}_e \mathcal{L}_e \mathcal{Q}_e)^{-1} \otimes I_{2m} \right] (\mathcal{Q}_e \mathcal{L}_e \mathcal{P}_e \otimes I_{2m} + \mathcal{Q} \mathcal{L}_{int} \mathcal{P}), \quad (B6)$$

where $\mathcal{P} = \mathcal{P}_e \otimes I_{2m}$ and $\mathcal{Q} = \mathcal{Q}_e \otimes I_{2m}$, with $\mathcal{P}_e = |\rho_e^{ss}\rangle\langle\rho_e^{ss}|$ and $\mathcal{Q}_e = I_{2e} - \mathcal{P}_e$. By applying these projectors in Eqs. (A2), (A5) and (A6), we obtain

$$\mathcal{P} \mathcal{L}_{int} \mathcal{P} = 0, \quad (B7)$$

$$\begin{aligned} \mathcal{P} \mathcal{L}_{int} \mathcal{Q} = -i \left[& |\rho_e^{ss}\rangle\langle\psi_3| \otimes (s_{ge}^\dagger \otimes I_m - I_m \otimes s_{ge}) + |\rho_e^{ss}\rangle\langle\psi_1| \otimes (s_{ge} \otimes I_m - I_m \otimes s_{ge}^\dagger) \right. \\ & \left. + |\rho_e^{ss}\rangle\langle\psi_6| \otimes (s_{gf}^\dagger \otimes I_m - I_m \otimes s_{gf}) + |\rho_e^{ss}\rangle\langle\psi_2| \otimes (s_{gf} \otimes I_m - I_m \otimes s_{gf}^\dagger) \right], \end{aligned} \quad (B8)$$

$$\mathcal{Q}_e \mathcal{L}_e \mathcal{P}_e = 0, \quad (B9)$$

and

$$\mathcal{Q} \mathcal{L}_{int} \mathcal{P} = -i (|\psi_3\rangle\langle I_e| \otimes s_{ge} \otimes I_m - |\psi_1\rangle\langle I_e| \otimes I_m \otimes s_{ge} + |\psi_6\rangle\langle I_e| \otimes s_{gf} \otimes I_m - |\psi_2\rangle\langle I_e| \otimes I_m \otimes s_{gf}). \quad (B10)$$

Furthermore, using Sympy, we have that

$$\begin{aligned} (\mathcal{Q}_e \mathcal{L}_e \mathcal{Q}_e)^{-1} = & -\frac{2}{\gamma_{ge}} |\psi_1\rangle\langle\psi_1| - \frac{2}{\gamma_{gf}} |\psi_2\rangle\langle\psi_2| - \frac{2}{\gamma_{ge}} |\psi_3\rangle\langle\psi_3| - \frac{1}{\gamma_{ge}} |\psi_4\rangle\langle\psi_4| \\ & - \frac{2}{\gamma_{ge} + \gamma_{gf}} |\psi_5\rangle\langle\psi_5| - \frac{2}{\gamma_{gf}} |\psi_6\rangle\langle\psi_6| - \frac{2}{\gamma_{ge} + \gamma_{gf}} |\psi_7\rangle\langle\psi_7| - \frac{1}{\gamma_{gf}} |\psi_8\rangle\langle\psi_8|. \end{aligned} \quad (B11)$$

Lastly, by replacing Eqs. (B7)-(B11) into Eq. (B6), we reach

$$\mathcal{L}_{eff} = \mathcal{P}_e \otimes \left[\mathcal{L}_m + \sum_{\alpha=ge,gf} \frac{2}{\gamma_\alpha} (2s_\alpha \otimes s_\alpha - s_\alpha^\dagger s_\alpha \otimes I_e - I_e \otimes s_\alpha^\dagger s_\alpha) \right], \quad (B12)$$

leading to Eq. (54).

[1] J. Gemmer, M. Michel, and G. Mahler, *Quantum Thermodynamics: Emergence of Thermodynamic Behavior Within Composite Quantum Systems*, 2nd ed., Lecture Notes in Physics (Springer Berlin, Heidelberg, 2009).

[2] F. Binder, L. Correa, C. Gogolin, J. Anders, and G. Adesso, *Thermodynamics in the Quantum Regime: Fundamental Aspects and New Directions*, 1st ed., Fundamental Theories of Physics (Springer Cham, 2019).

[3] T. D. Kieu, *Phys. Rev. Lett.* **93**, 140403 (2004).

[4] H. T. Quan, Y.-x. Liu, C. P. Sun, and F. Nori, *Phys. Rev. E* **76**, 031105 (2007).

[5] H. Wang, S. Liu, and J. He, *Phys. Rev. E* **79**, 041113 (2009).

[6] N. Linden, S. Popescu, and P. Skrzypczyk, *Phys. Rev. Lett.* **105**, 130401 (2010).

[7] M. O. Scully, K. R. Chapin, K. E. Dorfman, M. B. Kim, and A. Svidzinsky, *Proceedings of the National Academy of Sciences* **108**, 15097 (2011), <https://www.pnas.org/content/108/37/15097.full.pdf>.

[8] J. Wang, Z. Wu, and J. He, *Phys. Rev. E* **85**, 041148 (2012).

[9] S. Rahav, U. Harbola, and S. Mukamel, *Phys. Rev. A* **86**, 043843 (2012).

[10] D. Gelbwaser-Klimovsky, R. Alicki, and G. Kurizki, *Phys. Rev. E* **87**, 012140 (2013).

[11] J. Roßnagel, O. Abah, F. Schmidt-Kaler, K. Singer, and E. Lutz, *Phys. Rev. Lett.* **112**, 030602 (2014).

[12] R. Uzdin, A. Levy, and R. Kosloff, *Phys. Rev. X* **5**, 031044 (2015).

[13] M. Beau, J. Jaramillo, and A. Del Campo, *Entropy* **18**, 10.3390/e18050168 (2016).

[14] J. Roßnagel, S. T. Dawkins, K. N. Tolazzi, O. Abah, E. Lutz, F. Schmidt-Kaler, and K. Singer, *Science* **352**, 325 (2016), <https://www.science.org/doi/pdf/10.1126/science.aad6320>.

[15] S. Çakmak, F. Altintas, A. Gençten, and Ö. E. Müstecapoglu, *The European Physical Journal D* **71**, 75 (2017).

[16] R. Kosloff and Y. Rezek, *Entropy* **19**, 136 (2017).

[17] X. L. Huang, Y. F. Shang, D. Y. Guo, Q. Yu, and Q. Sun, *Quantum Information Processing* **16**, 174 (2017).

[18] L.-M. Zhao and G.-F. Zhang, *Quantum Information Pro-*

cessing **16**, 216 (2017).

[19] J. Klaers, S. Faelt, A. Imamoglu, and E. Togan, *Phys. Rev. X* **7**, 031044 (2017).

[20] K. Brandner, M. Bauer, and U. Seifert, *Phys. Rev. Lett.* **119**, 170602 (2017).

[21] W. Niedenzu, V. Mukherjee, A. Ghosh, A. G. Kofman, and G. Kurizki, *Nature Communications* **9**, 165 (2018).

[22] K. E. Dorfman, D. Xu, and J. Cao, *Phys. Rev. E* **97**, 042120 (2018).

[23] B. Xiao and R. Li, *Physics Letters A* **382**, 3051 (2018).

[24] B. Çakmak and O. E. Müstecaplıoğlu, *Phys. Rev. E* **99**, 032108 (2019).

[25] P. A. Camati, J. F. G. Santos, and R. M. Serra, *Phys. Rev. A* **99**, 062103 (2019).

[26] D. Türkpençe and F. Altintas, *Quantum Information Processing* **18**, 255 (2019).

[27] J. P. S. Peterson, T. B. Batalhão, M. Herrera, A. M. Souza, R. S. Sarthour, I. S. Oliveira, and R. M. Serra, *Phys. Rev. Lett.* **123**, 240601 (2019).

[28] R. J. de Assis, T. M. de Mendonça, C. J. Villas-Boas, A. M. de Souza, R. S. Sarthour, I. S. Oliveira, and N. G. de Almeida, *Phys. Rev. Lett.* **122**, 240602 (2019).

[29] D. von Lindenfels, O. Gräß, C. T. Schmiegelow, V. Kaushal, J. Schulz, M. T. Mitchison, J. Goold, F. Schmidt-Kaler, and U. G. Poschinger, *Phys. Rev. Lett.* **123**, 080602 (2019).

[30] J. Wang, J. He, and Y. Ma, *Phys. Rev. E* **100**, 052126 (2019).

[31] M. Wiedmann, J. T. Stockburger, and J. Ankerhold, *New Journal of Physics* **22**, 033007 (2020).

[32] J. Du, W. Shen, X. Zhang, S. Su, and J. Chen, *Phys. Rev. Res.* **2**, 013259 (2020).

[33] S. Çakmak and F. Altintas, *Quantum Information Processing* **19**, 248 (2020).

[34] T. Denzler and E. Lutz, *Phys. Rev. Res.* **2**, 032062 (2020).

[35] V. Singh and O. E. Müstecaplıoğlu, *Phys. Rev. E* **102**, 062123 (2020).

[36] Q. Bouton, J. Nettersheim, S. Burgardt, D. Adam, E. Lutz, and A. Widera, *Nature Communications* **12**, 2063 (2021).

[37] R. J. de Assis, J. S. Sales, U. C. Mendes, and N. G. de Almeida, *Journal of Physics B: Atomic, Molecular and Optical Physics* **54**, 095501 (2021).

[38] H. J. D. Miller, M. H. Mohammady, M. Perarnau-Llobet, and G. Guarnieri, *Phys. Rev. Lett.* **126**, 210603 (2021).

[39] W. S. Teixeira, M. K. Keller, and F. L. Semião, *New Journal of Physics* **24**, 023027 (2022).

[40] W. Ji, Z. Chai, M. Wang, Y. Guo, X. Rong, F. Shi, C. Ren, Y. Wang, and J. Du, *Phys. Rev. Lett.* **128**, 090602 (2022).

[41] S. Kamimura, H. Hakoshima, Y. Matsuzaki, K. Yoshida, and Y. Tokura, *Phys. Rev. Lett.* **128**, 180602 (2022).

[42] M. Kim, M. Scully, and A. Svidzinsky, *Nature Photonics* **16**, 669 (2022).

[43] S. Aimet and H. Kwon, *Phys. Rev. A* **107**, 012221 (2023).

[44] D. Das, G. Thomas, and A. N. Jordan, *Phys. Rev. A* **108**, 012220 (2023).

[45] F. Plastina, A. Alegre, T. J. G. Apollaro, G. Falcone, G. Francica, F. Galve, N. Lo Gullo, and R. Zambrini, *Phys. Rev. Lett.* **113**, 260601 (2014).

[46] D. Leibfried, R. Blatt, C. Monroe, and D. Wineland, *Rev. Mod. Phys.* **75**, 281 (2003).

[47] D. Finkelstein-Shapiro, D. Viennot, I. Saideh, T. Hansen, T. o. Pullerits, and A. Keller, *Phys. Rev. A* **101**, 042102 (2020).

[48] I. Saideh, D. Finkelstein-Shapiro, T. o. Pullerits, and A. Keller, *Phys. Rev. A* **102**, 032212 (2020).

[49] R. Srikanth and S. Banerjee, *Phys. Rev. A* **77**, 012318 (2008).

[50] P. Li and B. Jia, *Phys. Rev. E* **83**, 062104 (2011).

[51] A. Ghosh, S. S. Sinha, and D. S. Ray, *Phys. Rev. E* **86**, 011138 (2012).

[52] R. Alicki, *Journal of Physics A: Mathematical and General* **12**, L103 (1979).

[53] R. Kosloff, *The Journal of Chemical Physics* **80**, 1625 (1984), <https://doi.org/10.1063/1.446862>.

[54] H. Häffner, C. Roos, and R. Blatt, *Physics Reports* **469**, 155 (2008).

[55] R. Blatt and C. F. Roos, *Nature Physics* **8**, 277 (2012).

[56] J. Johansson, P. Nation, and F. Nori, *Computer Physics Communications* **183**, 1760 (2012).

[57] J. Johansson, P. Nation, and F. Nori, *Computer Physics Communications* **184**, 1234 (2013).